

Preliminary Draft Version

Fast Spectral Formulations of Thin Plate Laser Heating with GPU Implementation

1st Daniel Mejia-Parra^{†‡}, 2nd Ander Arbelaiz^{*‡§}, 3rd Aitor Moreno^{‡§},
4th Jorge Posada^{‡§}, 5th Oscar Ruiz-Salguero[†]

[†]Laboratory of CAD CAM CAE

Universidad EAFIT

Medellín, Colombia

[‡]Vicomtech Foundation

San Sebastián, Spain

[§]Basque Research and Technology Alliance (BRTA)

Mendaro, Spain

*Corresponding Author: aarbelaiz@vicomtech.org

Abstract—In the context of numerical methods, the problem of frequency-domain (spectral) simulations is crucial for the solution of Partial Differential Equations. Fast Fourier Transform (FFT) algorithms significantly reduce the computational cost of such simulations and enable parallelization using Graphics Processing Units (GPUs). In the particular subdomain of laser heating/cutting of rectangular metal plates, fast simulation is required for tool path planning, parameter optimization and additive manufacturing. The currently used methods include frequency-domain analytic solutions for single-beam and multi-beam laser heating. However, the problem of formulating these spectral problems in terms of Fourier methods and implementing them in efficient manner remains. To overcome these limitations, this article presents two different schemes that translate the problem of laser beam heating of metal plates into equivalent FFT problems. The results show significant improvements in terms of executions times, being 100× faster than current state-of-the-art algorithms. Future work needed involves the inclusion of stress analysis, complex plate geometries and non-constant material properties for the plate.

Index Terms—Fast Fourier Transform, Discrete Sine Transform, heat transfer, laser heating, thin metal plate, GPU

I. INTRODUCTION

Spectral analysis and spectral methods are competitive alternatives to numerical simulations of physical phenomena (e.g. acoustics, heat transfer, structural analysis and electromagnetism). Spectral methods provide frequency-domain solutions (infinite sum of trigonometric functions) to the Partial Differential Equations that model the aforementioned phenomena. The Discrete Fourier Transform (DFT) and the Fast Fourier Transform (FFT) are the key algorithms that retrieve the original spatial-based solution with low computational demand. The FFT is a widely used algorithm not only in the context of PDEs simulation, but also signal analysis and image processing.

In recent years, frequency-based methods have been developed for heat transfer simulation of the laser heating/cutting problem in rectangular plates. These solutions have shown to be significantly faster than standard numerical methods (such as Finite Element Methods) after some model simplifications.

They also allow to zoom into asynchronous time intervals without computing or storing the complete history of the solution. Fast simulation of laser heating/cutting problems is crucial for many different engineering problems, such as: tool path planning, laser parameter optimization, waste minimization, additive manufacturing, etc.

The aforementioned methods for laser heating/cutting simulation allow simulation of complex laser trajectories on the plate, and they even allow the introduction of multiple laser beams simultaneously. However, there are not, in the current state of the art, FFT-based solutions to the laser heating/cutting problem.

This manuscript presents two different schemes that cast the laser heating/cutting problem into a DST (Discrete Sine Transform) and DFT ones, respectively. Such a casting enables the use of FFT libraries both in CPU and GPU programming environments, significantly improving the efficiency of existing methods.

The remainder of this manuscript is organized as follows: Sect. II discusses the relevant literature. Sect. III presents the methodology. Sect. IV discusses the results. Finally, Sect. V presents the conclusions and discusses the future work.

II. LITERATURE REVIEW

A. Laser Heating/Cutting Simulation

Finite Element Analysis (FEA) is one of the most used methods for thermodynamic simulation of laser heating/cutting of metal plates. Using non-linear FEA, Ref. [1] simulates triangular cuts for residual stress analysis. Similarly, Refs. [2], [3] perform the same non-linear FEA analysis for rectangular cuts, and Ref. [4] studies circular cuts using the same approach. In order to account for laser ablation (material melting and evaporation), different methods such as enthalpy method [1]–[4], element birth and death [5], volume fractions [6], and temperature thresholds [7]–[9] have been presented.

Other numerical methods include Finite Differences [10]–[12], Boundary Elements [13], [14] and Finite Volumes [15],

[16]. However, numerical methods are computationally expensive in general, limiting their application to small plate geometries, simple laser trajectories, requiring full time history simulations.

Analytic methods provide significantly faster computations at the cost of some model simplifications. Ref. [17] presents a uni-dimensional analytic model for laser drilling processes when the laser beam is static. Ref [18] presents a solution for a moving laser on an infinite 2D plate. Ref. [19] presents a frequency-based solution for rectangular plates when the moving laser follows a straight path. Similarly, Refs. [20], [21] present a frequency-based solution for arbitrary laser trajectories. Finally, Ref. [22] extends the previous frequency-based solutions to multiple laser beams simultaneously heating the plate surface.

B. FFT-based Laser Heating Simulation

FFT-based methods are relevant in the solution of physical problems by solving the inherent Partial Differential Equation (PDE) in the frequency domain. As a consequence, these methods have been successfully implemented in the simulation of different physics phenomena. For example, in the context of heat transfer analysis, Ref. [23] presents an FFT based method for the solution of the thermoelastic equation on infinite domains, while Ref. [24] applies the FFT to the solution of a heat transfer problem that arises in treatments of tissue with cancer. In structural analysis, Refs. [25]–[28] develop FFT-based methods for the solution of different elasticity and plasticity problems, and Ref. [29] presents a FFT-based solver for fluid mechanics. Other applications of the FFT include electromagnetism [30], 1D signal processing [31], and 2D image processing [32].

As discussed previously, Refs. [19]–[22] solve the problem of laser heating simulation in the frequency domain. However, none of these references are able to cast their problems into the FFT domain.

C. Conclusions of the Literature Review

Current analytic methods for laser heating/cutting simulation already provide fast solutions to the problem in the frequency domain. However, these methods perform direct evaluation of the Fourier transform, whose computational complexity for a 2D plate becomes $\mathcal{O}(M^2 N^2)$ (with $M^2 \times N^2$ being the grid size that discretizes the rectangular plate). These applications are, therefore, computationally expensive.

To overcome such a problem, this manuscript presents 2 different schemes that cast the existing analytic solutions into equivalent DST and DFT problems, respectively. Mathematical proof for each scheme is presented. Afterwards, algorithms that make use of FFT libraries to solve each of these schemes are introduced, reducing the computational complexity of the problem to $\mathcal{O}(MN \log(MN))$. The algorithms are implemented both in CPU and GPU architectures. The test results show significant improvements to the current state of the art simulations (i.e. Ref. [21]), reducing the measured computation times from 1s to 0.01s (100× faster) for a

1024 × 1024 plate, and enabling simulations for larger plates (up to 4096 × 4096).

III. METHODOLOGY

A. Heat Transfer Equation for Laser Heating on Thin Plates

The temperature $u(x, y, t)$ (K) distribution on a 2D rectangular plate for a continuous laser beam source satisfies the following partial differential equation with initial and boundary conditions:

$$\begin{aligned} \frac{f - q}{\Delta z} &= \rho c_p \frac{\partial u}{\partial t} - \nabla \cdot (\kappa \nabla u) \\ q(x, y, t) &= h \cdot (u(x, y, t) - u_\infty) \\ u(x, y, 0) &= u_\infty \\ u(0, y, t) &= u(a, y, t) = u(x, 0, t) = u(x, b, t) = u_\infty \end{aligned} \quad (1)$$

where $a \times b \times \Delta z$ are the plate dimensions (m^3), ρ is the plate density (kg/m^3), c_p is the specific heat ($J/[kg K]$) and κ is the thermal conductivity ($W/[m K]$). $q = q(x, y, t)$ is the heat loss due to convection at the plate surface ($W/[m^2]$), h is the convection coefficient ($W/[m^2 K]$) and u_∞ is the ambient temperature (K). Finally, the heat source $f = f(x, y, t)$ ($W/[m^2 K]$) is defined as a square-shape moving laser beam:

$$f(x, y, t) = \begin{cases} \frac{P(1-R)}{\pi r^2}, & \max(|x - x_0(t)|, |y - y_0(t)|) < \frac{r\sqrt{\pi}}{2} \\ 0, & \text{otherwise} \end{cases} \quad (2)$$

where $0 \leq R < 1$ is the plate reflectivity, $P > 0$ is the laser power (W), $r > 0$ is the laser radius (m) and $\mathbf{x}_0(t) = [x_0(t), y_0(t)]$ is the location of the laser spot at time t . \mathbf{x}_0 is the parametric curve that defines the laser trajectory, discretized as a sequence of piecewise linear trajectories as described in [20], [21]. Fig. 1 presents an scheme of the laser heating problem on thin metal plates.

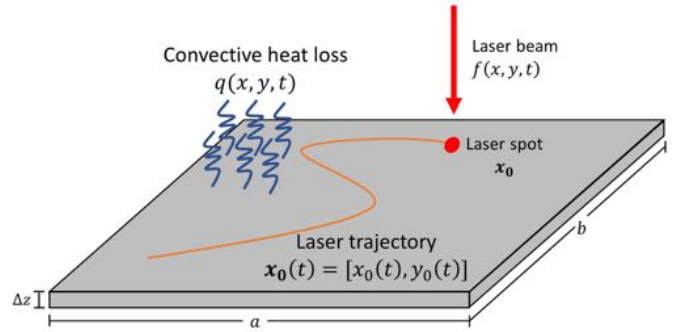


Fig. 1. Scheme for the laser heating problem on thin metal plates

B. Analytic Solution

According to Refs. [20], [21], the solution to Eq. (1) can be expressed as Fourier series:

$$u(x, y, t) = u_\infty + \sum_{m=0}^{\infty} \sum_{n=0}^{\infty} \theta_{mn}(t) \sin(\alpha_m x) \sin(\beta_n y) \quad (3)$$

with $\alpha_m = (m+1)\pi/a$ and $\beta_n = (n+1)\pi/b$. Each Fourier coefficient $\theta_{mn}(t)$ is defined as:

$$\theta_{mn}(t) = \frac{4}{ab\rho c_p \Delta z} \times \int_0^t \int_0^b \int_0^a f(x, y, \tau) \sin(\alpha_m x) \sin(\beta_n y) e^{-\omega_{mn}(t-\tau)} dx dy d\tau \quad (4)$$

with Laplace eigenvalues ω_{mn} :

$$\omega_{mn} = \frac{\kappa}{\rho c_p} (\alpha_m^2 + \beta_n^2) + \frac{h}{\rho c_p \Delta z} \quad (5)$$

Let $\mathbf{C}_1(t), \mathbf{C}_2(t), \dots$ be a sequence of piecewise linear sub-trajectories that discretize the complete laser trajectory, i.e. $\mathbf{x}_0(t) \approx \mathbf{C}_1(t), \mathbf{C}_2(t), \dots$. Each sub-trajectory \mathbf{C}_i ($i > 0$) is defined as follows:

$$\mathbf{C}_i(t) = \mathbf{x}_0(t_i) \frac{t - t_{i-1}}{t_i - t_{i-1}} + \mathbf{x}_0(t_{i-1}) \frac{t_i - t}{t_i - t_{i-1}}, \quad t_{i-1} \leq t < t_i \quad (6)$$

where the original laser trajectory \mathbf{x}_0 is sampled at $t = t_0, t_1, t_2, \dots$.

The analytic solution for Eq. (4) for the given piecewise linear discretization is presented in Refs. [20], [21].

C. Discrete Fourier Transform (DFT) and Fast Fourier Transform (FFT)

The Discrete Fourier Transform (DFT) [33] allows to write any sequence of M real numbers as a finite sum of sine and cosine functions, i.e. a Fourier series. The (1D) DFT of the sequence of real values $G = \{g_0, g_1, \dots, g_{M-1}\} \subset \mathbb{R}$ is defined as:

$$g_k = \sum_{m=0}^{M-1} \phi_m e^{-\frac{i2\pi}{M} km} = \sum_{m=0}^{M-1} \phi_m \left[\cos \frac{2\pi km}{M} - i \sin \frac{2\pi km}{M} \right] \quad (7)$$

where $\phi_m \in \mathcal{C}$ is the m^{th} Fourier coefficient and $i = \sqrt{-1}$ is the imaginary unit.

The computational complexity for direct evaluation of Eq. (7) is $\mathcal{O}(M^2)$. The Fast Fourier Transform (FFT) [31] is an algorithm that eliminates redundant arithmetic computations that arise due to the symmetries of the sine and cosine functions in Eq. (7). As a consequence, the FFT algorithm reduces the computational complexity of the problem to $\mathcal{O}(M \log M)$ [31].

The above DFT and FFT complexity orders are true for 1D arrays. Therefore, for a 2D discrete plate of size $M \times N$, the computational complexities become $\mathcal{O}(M^2 \times N^2)$ and $\mathcal{O}(MN \log(MN))$ for the DFT and the FFT, respectively.

The remainder of this section describes how to cast Eq. (3) as a DFT problem and therefore, solve it using any FFT algorithm. This casting effectively improves the computational complexity of the problem with respect to the current state of the art [20]–[22].

D. Scheme 1 - Discrete Sine Transform (DST)

The Discrete Sine Transform (DST) [34] is a particular case of the DFT transform in which only the sine terms of the Fourier series are considered. The (1D) DFT of the sequence $G = \{g_0, g_1, \dots, g_{M-1}\} \subset \mathcal{R}$ is defined as:

$$g_k = \sum_{m=0}^{M-1} \phi_k \sin \frac{(m+1)(k+1)\pi}{M+1} \quad (8)$$

Intuitively, this is the easiest of the schemes for casting the problem as Eq. (3) only considers the sine terms of a Fourier series. The mathematical proof of such a casting and the algorithm for the retrieval of the plate temperature is discussed below.

1) *Mathematical Proof:* Let $\{x_0, x_1, \dots, x_M\}$ and $\{y_0, y_1, \dots, y_N\}$ be uniform discretizations of the intervals $[0, a]$ and $[0, b]$, respectively. It is worth noting that for such a uniform sampling, the equalities $x_k/a = i/M$ and $y_l/b = l/N$ hold. Therefore, after truncating the number of Fourier coefficients to $(M-1) \times (N-1)$, Eq. (3) is approximated as:

$$u_{kl}(t) = u_\infty + \sum_{m=0}^{M-2} \sum_{n=0}^{N-2} \theta_{mn} \sin(\gamma_{m+1}k) \sin(\delta_{n+1}l), \quad (9)$$

$$k = 0, 1, \dots, M, \quad l = 0, 1, \dots, N$$

with $u_{kl}(t) = u(x_k, y_l, t)$ the temperature at the discrete points of the plate and $\gamma_m = m\pi/M$, $\delta_n = n\pi/N$ the discrete versions of α_m and β_n , respectively. This equation is equivalent to a 2D DST of the temperatures on the discrete plate (as per Eq. (8)).

2) *Algorithm:* Algorithm 1 presents the algorithm used to retrieve the temperature defined in Eq. (9) at any given time t with the DST method. Line 2 applies the 2D DST of any FFT library, while Line 3 applies the initial and boundary conditions presented in Eq. (1) to the computed solution. The complexity of the presented algorithm is $\mathcal{O}(MN \log(MN))$.

Algorithm 1 Retrieve temperature using a 2D DST

Require: $\Theta \in \mathbb{R}^{(M-2) \times (N-2)}$, $u_\infty \in \mathbb{R}$

Ensure: $U \in \mathbb{R}^{M \times N}$

- 1: $U \leftarrow \text{zeros}(M, N)$
 - 2: $U[1 : M-1, 1 : N-1] \leftarrow \text{dst2d}(\Theta)$
 - 3: $U \leftarrow U + u_\infty$
 - 4: **return** U
-

E. Scheme 2 - Fast Fourier Transform (FFT)

In this scheme, the original list of Fourier coefficients is duplicated in size in each direction ($2M \times 2N$). The idea is to take advantage of the odd symmetry of the sine function at $k\pi$ (with $k \in \mathbb{N}_+$). Therefore, the added coefficients are set by mirroring the original M or N coefficients (multiplied by -1) in each direction. The final temperature is obtained from the imaginary (sine) components of the FFT result.

1) *Mathematical Proof:* Consider $\{x_0, x_1, \dots, x_M\}$ be a uniform discretization of the interval $[0, a]$. Since $\sin(x) = -\sin(-x)$ and $\sin(x) = \sin(x + 2k\pi)$ (with $k \in \mathbb{N}_+$) the following equation holds:

$$\begin{aligned}
& \sum_{m=0}^{M-2} \theta_{mn} \sin \frac{(m+1)k\pi}{M} \\
&= - \sum_{m=0}^{M-2} \theta_{mn} \sin \frac{-(m+1)k\pi}{M} \\
&= - \sum_{m=0}^{M-2} \theta_{mn} \sin \left(\frac{-(m+1)k\pi}{M} + 2k\pi \right) \\
&= - \sum_{m=0}^{M-2} \theta_{mn} \sin \left(\frac{(2M-m-1)k\pi}{M} \right), \\
& n = 0, 1, \dots, N
\end{aligned} \tag{10}$$

The previous series can be expressed in reverse form by setting $m \leftarrow M - m - 2$:

$$\begin{aligned}
& \sum_{m=0}^{M-2} \theta_{mn} \sin \frac{(m+1)k\pi}{M} \\
&= - \sum_{m=0}^{M-2} \theta_{(M-m-2)n} \sin \left(\frac{(M+m+1)k\pi}{M} \right)
\end{aligned} \tag{11}$$

Afterwards, consider the sequence shift $m = M + 1, M + 2, \dots, 2M - 1$. Eq. (11) becomes:

$$\begin{aligned}
& \sum_{m=0}^{M-2} \theta_{mn} \sin \frac{(m+1)k\pi}{M} \\
&= - \sum_{m=M+1}^{2M-1} \theta_{(2M-m-1)n} \sin \left(\frac{mk\pi}{M} \right)
\end{aligned} \tag{12}$$

which is the second half of a sine transform with negative coefficients in reverse order. Therefore, the series can be split in two as follows:

$$\begin{aligned}
& \sum_{m=0}^{M-2} \theta_{mn} \sin \frac{(m+1)k\pi}{M} \\
&= \frac{1}{2} \sum_{m=0}^{M-2} \theta_{mn} \sin \frac{(m+1)k\pi}{M} \\
&+ \frac{1}{2} \sum_{m=M+1}^{2M-1} -\theta_{(2M-m-1)n} \sin \left(\frac{mk\pi}{M} \right)
\end{aligned} \tag{13}$$

On the other hand, from Eq. (7):

$$\begin{aligned}
\phi_m \sin \frac{mk\pi}{M} &= -\mathcal{I} \left[-\phi_m^i \sin \frac{2mk\pi}{2M} \right] \\
&= -\mathcal{I} \left[\phi_m e^{-\frac{i2\pi}{2M} km} \right]
\end{aligned} \tag{14}$$

where $\mathcal{I}[\cdot]$ corresponds to the complex component of the Fourier term.

Putting together Eqs. (13) and (14), Eq. (3) becomes:

$$\begin{aligned}
u_{kl}(t) &= u_\infty \\
&+ \frac{1}{4} \mathcal{I} \left[\sum_{n=0}^{N-2} \mathcal{I} \left[\sum_{m=0}^{M-2} \theta_{mn} e^{-\frac{i2\pi}{2M} k(m+1)} \right] e^{-\frac{i2\pi}{2N} l(n+1)} \right] \\
&- \frac{1}{4} \mathcal{I} \left[\sum_{n=0}^{N-2} \mathcal{I} \left[\sum_{m=M+1}^{2M-1} \theta_{(2M-m-1)n} e^{-\frac{i2\pi}{2M} km} \right] e^{-\frac{i2\pi}{2N} l(n+1)} \right] \\
&- \frac{1}{4} \mathcal{I} \left[\sum_{n=N+1}^{2N-1} \mathcal{I} \left[\sum_{m=0}^{M-2} \theta_{m(2N-n-1)} e^{-\frac{i2\pi}{2M} k(m+1)} \right] e^{-\frac{i2\pi}{2N} ln} \right] \\
&+ \frac{1}{4} \mathcal{I} \left[\sum_{n=N+1}^{2N-1} \mathcal{I} \left[\sum_{m=M+1}^{2M-1} \theta_{(2M-m-1)(2N-n-1)} e^{-\frac{i2\pi}{2M} km} \right] e^{-\frac{i2\pi}{2N} ln} \right] \\
& k = 0, 1, \dots, M, \quad l = 0, 1, \dots, N
\end{aligned} \tag{15}$$

The previous equation is equivalent to 2 nested 1D DFTs (Eq. (7)) after padding the $M - 2$ coefficients in reverse order (and negative) at the end of the original Fourier coefficients in each direction (x and y), respectively.

2) *Algorithm:* Algorithm 2 presents the algorithm used to retrieve the temperature of Eq. (15) at any given time t using the FFT. Line 1 initializes the extended matrix of Fourier coefficients with M, N trailing zeros. Lines 3-5 and Lines 6-8 add the reversed sequences of Fourier coefficients (with negative sign) in each dimension, respectively. Lines 10 and 14 compute the 1D FFT of the padded arrays for the y and x dimensions, respectively. Lines 11 and 15 extract the complex (imaginary component) of the results. Finally, Line 12 removes the mirrored part from solution while Line 13 applies initial and boundary conditions. The complexity of the presented algorithm is $\mathcal{O}(MN \log(MN))$.

IV. RESULTS

This section presents the results of the implementation of Algorithms 1 and 2 using different state-of-the-art FFT libraries for the solution of the laser heating problem on thin metal plates. All the simulations are executed with the same parameters and laser trajectory presented in [21] (see Table I). Section IV-A presents the numerical validation of the presented schemes with respect to the state of the art analytic algorithms [21]. Finally, Section IV-B discusses the computational performance of the proposed algorithms using available FFT libraries.

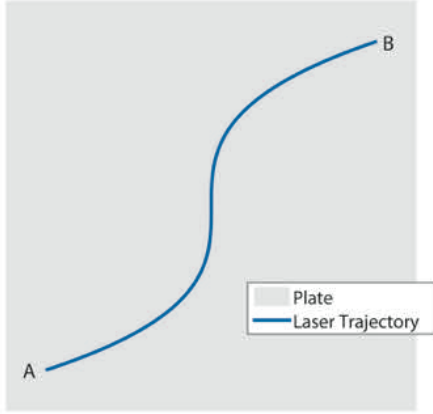
A. Numerical Validation

Sect. III validates the correctness of the presented schemes. However, a numerical validation is presented in this section with numerical and graphical results for the already mentioned test case. Fig. 2(a) plots the laser trajectory on the plate. Fig. 2(b) plots the temperature distribution results obtained with the method presented in [21].

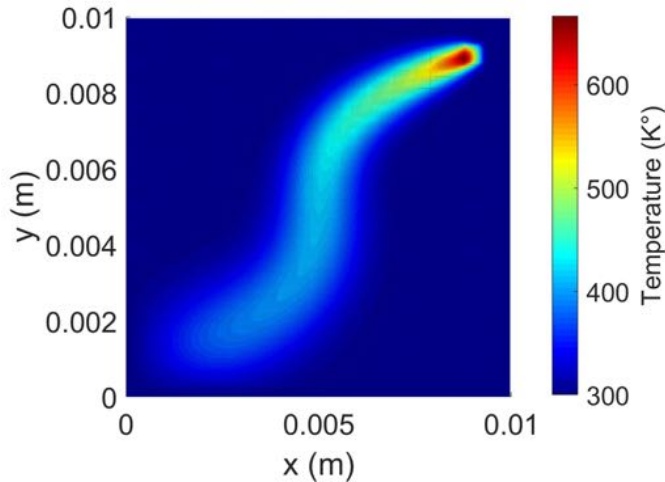
Fig. 3(a) presents the simulation results using the DST algorithm for a 1024×1024 thin metal plate. Fig. 3(b) plots the absolute error measured with respect to the analytic

TABLE I
PARAMETERS FOR THE PHYSICAL SIMULATION

Parameter	Description	Value	Units
a	Plate width	0.01	m
b	Plate height	0.01	m
Δz	Plate thickness	0.01	m
ρ	Plate density	8030	kg/m^3
c_p	Specific heat	574	$J/(kg K)$
κ	Thermal conductivity	20	$W/(m K)$
R	Plate reflectivity	0	1
h	Convection coefficient	20	$W/(m^2 K)$
u_∞	Ambient temperature	300	K
P	Laser power	100	W
r	Laser spot radius	0.0003	m



(a) Laser trajectory for the simulation



(b) Analytic temperature solution [21]

Fig. 2. Laser trajectory and analytic simulation results for the method presented in [21]

Algorithm 2 Retrieve temperature using a FFT by mirroring the original coefficients

Require: $\Theta \in \mathbb{R}^{(M-2) \times (N-2)}$, $u_\infty \in \mathbb{R}$

Ensure: $U \in \mathbb{R}^{M \times N}$

```

1:  $\Theta_{MIRRORED} \leftarrow \text{zeros}(2M, 2N)$ 
2:  $\Theta_{MIRRORED}[1 : M - 1, 1 : M - 1] \leftarrow \Theta$ 
3: for  $m = M + 1, m < 2M - 1, m \leftarrow m + 1$  do
4:    $\Theta_{MIRRORED}[m, :] \leftarrow -\Theta_{MIRRORED}[2M - m - 1]$ 
5: end for
6: for  $n = N + 1, n < 2N - 1, n \leftarrow n + 1$  do
7:    $\Theta_{MIRRORED}[n, :] \leftarrow -\Theta_{MIRRORED}[2N - n - 1]$ 
8: end for
9: for  $n = 1, n < N - 1, n \leftarrow n + 1$  do
10:   $arr \leftarrow \text{fft}(\Theta_{MIRRORED}[:, n])$ 
11:   $\Theta_{MIRRORED}[:, n] \leftarrow \text{imag}(arr)$ 
12: end for
13: for  $m = 1, m < M - 1, m \leftarrow m + 1$  do
14:   $arr \leftarrow \text{fft}(\Theta_{MIRRORED}[m, :])$ 
15:   $\Theta_{MIRRORED}[m, :] \leftarrow \text{imag}(arr)$ 
16: end for
17:  $U \leftarrow \text{zeros}(M, N)$ 
18:  $U \leftarrow \Theta_{MIRRORED}[0 : M - 1, 0 : N - 1]$ 
19:  $U \leftarrow U + u_\infty$ 
20: return  $U$ 

```

solution presented in Fig. 2(b). The resulting error is negligible ($< 10^{-11}(K)$), and evenly distributed along the 2D plate. Similarly, Fig. 3(c) plots the temperature distribution using the FFT for the same 1024×1024 plate. In this case, the error also stays below $10^{-11}(K)$ (see Fig. 3(d)).

B. Computational performance

This section evaluates the performance of the proposed methods under CPU and GPU hardware by making use of highly optimized libraries. The Python programming language and its scientific package ecosystem contains high level wrappers to C/C++ libraries. For this reason, Python has been selected for the rapid prototyping of the proposed methods. The performance differences between libraries, as well as the speed-up against the state of the art analytic solution have been measured.

The FFT algorithm is used in a wide range of performance demanding applications. Therefore, the optimization degree of its implementation is highly relevant. On the one hand, to target the CPU, the FFTPACK, MKL and FFTW libraries have been selected. On the other hand, to target the GPU, the cuFFT library from the NVIDIA CUDA Toolkit has been used. All these libraries make use of multi-core parallelization, vectorization instructions, efficient memory usage and apply specific FFT algorithms to exploit the underlying hardware to the highest degree.

Table II summarizes the selected libraries along the Python wrapper packages and the targeted hardware device during the performance tests.

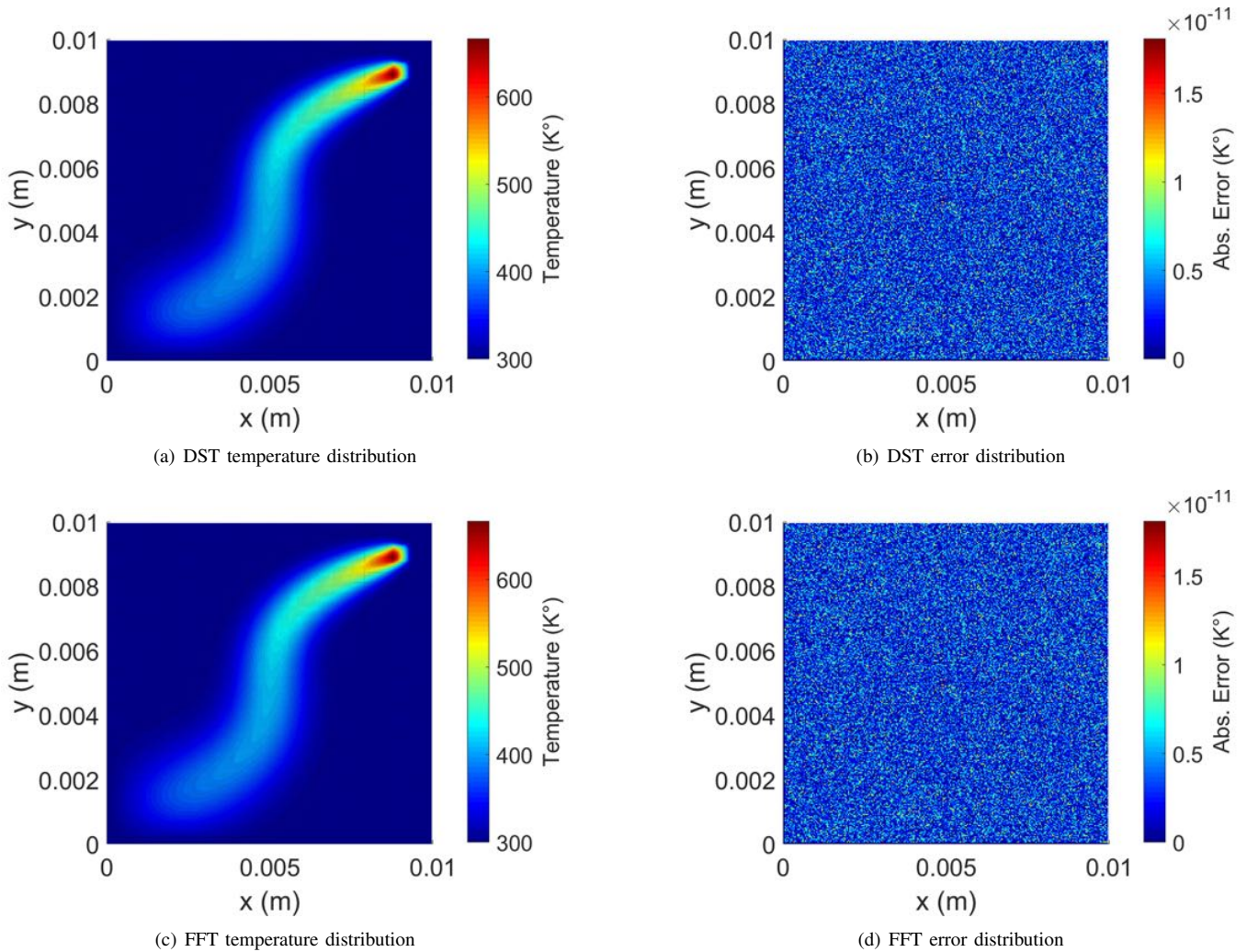


Fig. 3. Temperature and absolute error distributions (w.r.t. [21]) on the thin plates for the DST and FFT approaches

TABLE II
PARAMETERS FOR THE PHYSICAL SIMULATION

Library	Package	Hardware
FFTPACK	scipy.fftpack	CPU
MKL	numpy.fft	CPU
FFTW	pyfftw	CPU
cuFFT	pyCUDA, scikit-cuda	GPU

The test platform used for the measurements is the following: a desktop PC using Windows 10 with an Intel Core i5-6500 (CPU), 16 GB RAM and NVIDIA GeForce GTX 960 (GPU). To measure the execution times of each method, each test has been computed 5 times and the minimum time has been registered.

Fig. 4 shows the computation time for both the proposed DST (FFTPACK only) and FFT (FFTPACK, MKL, FFTW and cuFFT) methods. The DST implementation available in FFFPACK is efficient for plate discretization sizes below 512×512 . Above this size, the FFT based method is much

even within FFFPACK. Between FFFPACK, MKL and FFTW, the optimization degree achieved for the FFT with the last two is higher. Results obtained with the FFTW library are slightly better (faster) than the MKL ones, but this can be due to the usage of wrappers, as the *pyfftw* wrapper offers more control over the FFTW implementation. Both, FFTW and MKL have shown very good performance results with execution times under 1s for plate sizes up to 4096×4096 . The cuFFT library that makes use of GPU hardware has shown the best performance results for sizes $\geq 1024 \times 1024$.

Fig. 5 compares the performance between CPU and GPU under the test platform for the FFT method. As the Fourier coefficients can be computed in the GPU before performing the temperature computation, the input for the FFT is already in GPU memory. Thus, the transfer of these coefficients from host memory (CPU) to device memory (GPU) is not measured. This comparison shows that the GPU hardware effectively accelerates the computation time nearly to a $2\times$ speed-up for sizes $\geq 1024 \times 1024$.

Fig. 6 compares the proposed FFT method with the state of

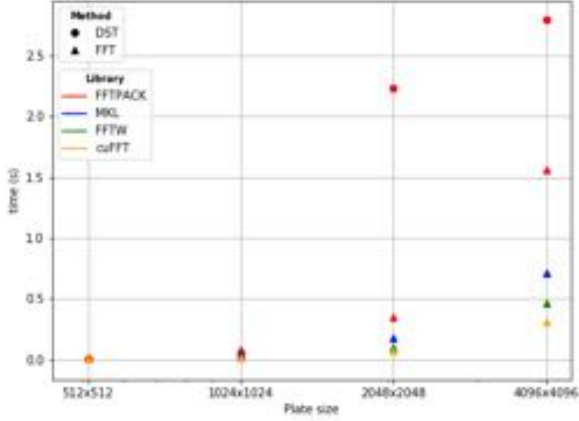


Fig. 4. Execution times for the DST and FFT for different plate resolutions using the libraries presented in Table II

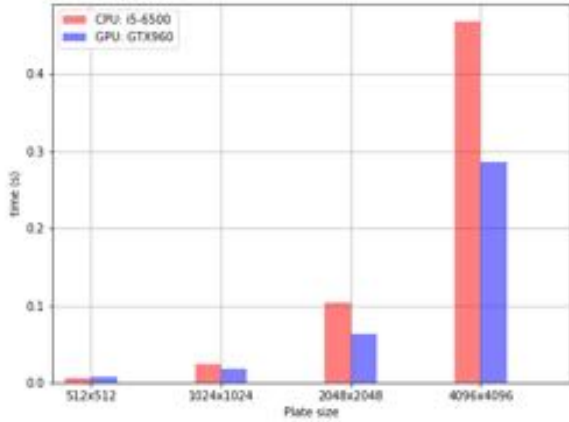


Fig. 5. Comparison of CPU vs GPU execution times for the FFT with different plate resolutions

the art GPU analytic solution [21]. The presented FFT method is much faster for plate sizes $> 128 \times 128$, showing a big gap in performance with a plate of size 1024×1024 where the FFT approach obtains a $124\times$ speed-up ($2.255138s$ against $0.018186s$). Fig. 6 demonstrates the potential of the presented FFT method to perform the temperature evaluation for high resolution plate sizes of 1024×1024 and beyond. Furthermore, the current analytic solution [21] has a limit size of 1024×1024 due to GPU shared memory usage, while the proposed FFT approach can compute the temperature for plates of sizes up to 4096×4096 under the same GPU hardware, without resorting to out of GPU memory management. For small plate sizes ($\leq 128 \times 128$), the analytic approach is faster because the FFT method requires extra processing of input coefficients and dispatching of kernels (scheduling time), adding a small computation overhead.

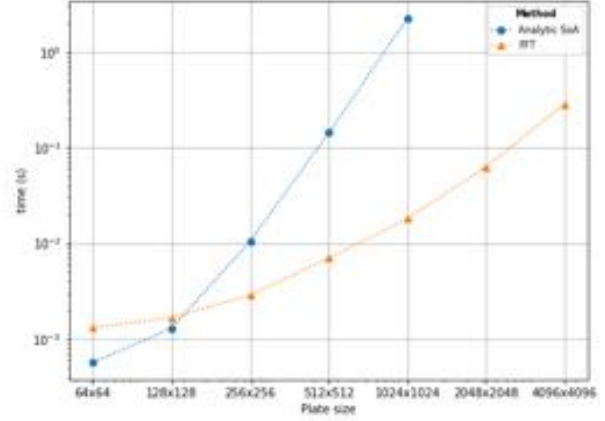


Fig. 6. Appraisal of the computation times (in GPU) for the presented FFT method vs the analytic method presented in [21]

V. CONCLUSIONS AND FUTURE WORK

This manuscript presents two different schemes for the solution of the laser heating problem on thin metal plates using the DST and the FFT. The presented methods improve the computational complexity of the problem from $\mathcal{O}(M^2N^2)$ to $\mathcal{O}(MN \log(MN))$ (with $M \times N$ being the discretization size of the metal plate). These methods are implemented in both CPU and GPU architectures using available FFT libraries in the Python programming language. Mathematical and numerical proofs of the correctness of the schemes are presented and the numerical error is measured below $10^{-11} K$. The computation times for the temperature evaluation are reduced from $1s$ to $0.01s$ ($100\times$ faster), measured in an NVIDIA GeForce GTX 960 (GPU).

Future work includes (1) the inclusion of thermal/stress models for structural analysis of the plate after the generated high temperature gradients, (2) analysis of non-rectangular plate geometries, and (3) consideration of non-linear interactions such as temperature-dependent thermal properties and phase changes.

REFERENCES

- [1] B. S. Yilbas, S. Akhtar, and O. Keles, "Laser cutting of triangular blanks from thick aluminum foam plate: Thermal stress analysis and morphology," *Applied Thermal Engineering*, vol. 62, no. 1, pp. 28 – 36, 2014. [Online]. Available: <http://www.sciencedirect.com/science/article/pii/S1359431113006601>
- [2] S. Akhtar, O. O. Kardas, O. Keles, and B. S. Yilbas, "Laser cutting of rectangular geometry into aluminum alloy: Effect of cut sizes on thermal stress field," *Optics and Lasers in Engineering*, vol. 61, pp. 57 – 66, 2014. [Online]. Available: <http://www.sciencedirect.com/science/article/pii/S0143816614001110>
- [3] B. Yilbas, S. Akhtar, and C. Karatas, "Laser cutting of rectangular geometry into alumina tiles," *Optics and Lasers in Engineering*, vol. 55, pp. 35 – 43, 2014. [Online]. Available: <http://www.sciencedirect.com/science/article/pii/S0143816613003047>
- [4] S. S. Akhtar, "Laser cutting of thick-section circular blanks: thermal stress prediction and microstructural analysis," *The International Journal of Advanced Manufacturing Technology*, vol. 71, no. 5, pp. 1345–1358,

- Mar 2014. [Online]. Available: <https://doi.org/10.1007/s00170-013-5594-5>
- [5] I. Roberts, C. Wang, R. Esterlein, M. Stanford, and D. Mynors, "A three-dimensional finite element analysis of the temperature field during laser melting of metal powders in additive layer manufacturing," *International Journal of Machine Tools and Manufacture*, vol. 49, no. 12, pp. 916 – 923, 2009. [Online]. Available: <http://www.sciencedirect.com/science/article/pii/S0890695509001400>
 - [6] B. Shi and H. Attia, "Integrated Process of Laser-Assisted Machining and Laser Surface Heat Treatment," *Journal of Manufacturing Science and Engineering*, vol. 135, no. 6, 11 2013, 061021. [Online]. Available: <https://doi.org/10.1115/1.4025832>
 - [7] R. Akarapu, B. Q. Li, and A. Segall, "A thermal stress and failure model for laser cutting and forming operations," *Journal of Failure Analysis and Prevention*, vol. 4, no. 5, pp. 51–62, Oct 2004. [Online]. Available: <https://doi.org/10.1361/15477020420756>
 - [8] K. Y. Nyon, C. Y. Nyeoh, M. Mokhtar, and R. Abdul-Rahman, "Finite element analysis of laser inert gas cutting on inconel 718," *The International Journal of Advanced Manufacturing Technology*, vol. 60, no. 9, pp. 995–1007, Jun 2012. [Online]. Available: <https://doi.org/10.1007/s00170-011-3655-1>
 - [9] C. Fu, M. Sealy, Y. Guo, and X. Wei, "Finite element simulation and experimental validation of pulsed laser cutting of nitinol," *Journal of Manufacturing Processes*, vol. 19, pp. 81 – 86, 2015. [Online]. Available: <http://www.sciencedirect.com/science/article/pii/S15266125997000493>
 - [10] M. F. Modest, "Three-dimensional, transient model for laser machining of ablating/decomposing materials," *International Journal of Heat and Mass Transfer*, vol. 39, no. 2, pp. 221 – 234, 1996. [Online]. Available: <http://www.sciencedirect.com/science/article/pii/001793109500134U>
 - [11] G. chan Han and S. joo Nas, "A study on torch path planning in laser cutting processes part 1: Calculation of heat flow in contour laser beam cutting," *Journal of Manufacturing Processes*, vol. 1, no. 1, pp. 54 – 61, 1999, special Issue of the Journal of Manufacturing Systems. [Online]. Available: <http://www.sciencedirect.com/science/article/pii/S1526612599700058>
 - [12] W. Xu, J. Fang, X. Wang, T. Wang, F. Liu, and Z. Zhao, "A numerical simulation of temperature field in plasma-arc forming of sheet metal," *Journal of Materials Processing Technology*, vol. 164-165, pp. 1644 – 1649, 2005, aMPT/AMME05 Part 2. [Online]. Available: <http://www.sciencedirect.com/science/article/pii/S092401360500141X>
 - [13] M. J. Kim, "Transient evaporative laser-cutting with boundary element method," *Applied Mathematical Modelling*, vol. 25, no. 1, pp. 25 – 39, 2000. [Online]. Available: <http://www.sciencedirect.com/science/article/pii/S0307904X00000342>
 - [14] —, "Transient evaporative laser cutting with moving laser by boundary element method," *Applied Mathematical Modelling*, vol. 28, no. 10, pp. 891 – 910, 2004. [Online]. Available: <http://www.sciencedirect.com/science/article/pii/S0307904X04000356>
 - [15] K. Kheloufi, E. Hachemi Amara, and A. Benzaoui, "Numerical Simulation of Transient Three-Dimensional Temperature and Kerf Formation in Laser Fusion Cutting," *Journal of Heat Transfer*, vol. 137, no. 11, 06 2015, 112101. [Online]. Available: <https://doi.org/10.1115/1.4030658>
 - [16] P. Yuan and D. Gu, "Molten pool behaviour and its physical mechanism during selective laser melting of TiC/AlSi10mg nanocomposites: simulation and experiments," *Journal of Physics D: Applied Physics*, vol. 48, no. 3, p. 035303, jan 2015.
 - [17] K. Zimmer, "Analytical solution of the laser-induced temperature distribution across internal material interfaces," *International Journal of Heat and Mass Transfer*, vol. 52, no. 1, pp. 497 – 503, 2009. [Online]. Available: <http://www.sciencedirect.com/science/article/pii/S0017931008003827>
 - [18] M. F. Modest and H. Abakians, "Evaporative Cutting of a Semi-infinite Body With a Moving CW Laser," *Journal of Heat Transfer*, vol. 108, no. 3, pp. 602–607, 08 1986. [Online]. Available: <https://doi.org/10.1115/1.3246978>
 - [19] H.-J. Jiang and H.-L. Dai, "Effect of laser processing on three dimensional thermodynamic analysis for hsla rectangular steel plates," *International Journal of Heat and Mass Transfer*, vol. 82, pp. 98 – 108, 2015. [Online]. Available: <http://www.sciencedirect.com/science/article/pii/S0017931014009697>
 - [20] D. Mejia, A. Moreno, A. Arbelaz, J. Posada, O. Ruiz-Salguero, and R. Chopitea, "Accelerated Thermal Simulation for Three-Dimensional Interactive Optimization of Computer Numeric Control Sheet Metal Laser Cutting," *Journal of Manufacturing Science and Engineering*, vol. 140, no. 3, 12 2017, 031006. [Online]. Available: <https://doi.org/10.1115/1.4038207>
 - [21] D. Mejia-Parra, A. Moreno, J. Posada, O. Ruiz-Salguero, I. nigo Barandiaran, J. C. Poza, and R. Chopitea, "Frequency-domain analytic method for efficient thermal simulation under curved trajectories laser heating," *Mathematics and Computers in Simulation*, vol. 166, pp. 177 – 192, 2019. [Online]. Available: <http://www.sciencedirect.com/science/article/pii/S0378475419301557>
 - [22] D. Mejia-Parra, D. Montoya-Zapata, A. Arbelaz, A. Moreno, J. Posada, and O. Ruiz-Salguero, "Fast analytic simulation for multi-laser heating of sheet metal in gpu," *Materials*, vol. 11, no. 11, p. 2078, Oct 2018. [Online]. Available: <http://dx.doi.org/10.3390/ma11112078>
 - [23] Y. Ju and T. N. Farris, "FFT Thermoelastic Solutions for Moving Heat Sources," *Journal of Tribology*, vol. 119, no. 1, pp. 156–162, 01 1997. [Online]. Available: <https://doi.org/10.1115/1.2832452>
 - [24] J.-L. Dillenseger and S. Esneault, "Fast fit-based bioheat transfer equation computation," *Computers in Biology and Medicine*, vol. 40, no. 2, pp. 119 – 123, 2010. [Online]. Available: <http://www.sciencedirect.com/science/article/pii/S0010482509002030>
 - [25] S. Berbenni, V. Taupin, K. S. Djaka, and C. Fressengeas, "A numerical spectral approach for solving elasto-static field dislocation and g-disclination mechanics," *International Journal of Solids and Structures*, vol. 51, no. 23, pp. 4157 – 4175, 2014. [Online]. Available: <http://www.sciencedirect.com/science/article/pii/S0020768314003138>
 - [26] K. S. Djaka, A. Villani, V. Taupin, L. Capolungo, and S. Berbenni, "Field dislocation mechanics for heterogeneous elastic materials: A numerical spectral approach," *Computer Methods in Applied Mechanics and Engineering*, vol. 315, pp. 921 – 942, 2017. [Online]. Available: <http://www.sciencedirect.com/science/article/pii/S0045782516304741>
 - [27] R. Ma and T. J. Truster, "Fit-based homogenization of hypoelastic plasticity at finite strains," *Computer Methods in Applied Mechanics and Engineering*, vol. 349, pp. 499 – 521, 2019. [Online]. Available: <http://www.sciencedirect.com/science/article/pii/S0045782519301082>
 - [28] C. Paramtmuni and A. K. Kanjarla, "A crystal plasticity fit based study of deformation twinning, anisotropy and micromechanics in hcp materials: Application to az31 alloy," *International Journal of Plasticity*, vol. 113, pp. 269 – 290, 2019. [Online]. Available: <http://www.sciencedirect.com/science/article/pii/S0749641918303851>
 - [29] J. Starn, "A simple fluid solver based on the fft," *Journal of Graphics Tools*, vol. 6, no. 2, pp. 43–52, 2001. [Online]. Available: <https://doi.org/10.1080/10867651.2001.10487540>
 - [30] J. M. Taboada, L. Landesa, F. Obelleiro, J. L. Rodriguez, J. M. Bertolo, M. G. Araujo, J. C. Mourão, and A. Gomez, "High scalability fmm-fft electromagnetic solver for supercomputer systems," *IEEE Antennas and Propagation Magazine*, vol. 51, no. 6, pp. 20–28, Dec 2009.
 - [31] D. F. ELLIOTT, "Chapter 7 - fast fourier transforms," in *Handbook of Digital Signal Processing*, D. F. Elliott, Ed. San Diego: Academic Press, 1987, pp. 527 – 631. [Online]. Available: <http://www.sciencedirect.com/science/article/pii/B9780080507804500126>
 - [32] O. Raaf and A. E. H. Adane, "Pattern recognition filtering and bidimensional fft-based detection of storms in meteorological radar images," *Digital Signal Processing*, vol. 22, no. 5, pp. 734 – 743, 2012. [Online]. Available: <http://www.sciencedirect.com/science/article/pii/S1051200412000802>
 - [33] D. F. ELLIOTT, "Chapter 1 - transforms and transform properties," in *Handbook of Digital Signal Processing*, D. F. Elliott, Ed. San Diego: Academic Press, 1987, pp. 1 – 53. [Online]. Available: <http://www.sciencedirect.com/science/article/pii/B9780080507804500060>
 - [34] V. Britanak, P. C. Yip, and K. Rao, "Chapter 1 - discrete cosine and sine transforms," in *Discrete Cosine and Sine Transforms*, V. Britanak, P. C. Yip, and K. Rao, Eds. Oxford: Academic Press, 2007, pp. 1 – 15. [Online]. Available: <http://www.sciencedirect.com/science/article/pii/B9780123736246500035>